Rotational population and alignment distributions for inelastic scattering and trapping/desorption of NO on Pt(111)

D. C. Jacobs,[a] K. W. Kolasinski, S. F. Shane, and R. N. Zare
Department of Chemistry, Stanford University, Stanford, California 94305

(Received 19 December 1988; accepted 22 May 1989)

Rotationally resolved experiments on the NO/Pt(111) system explore the mechanisms of inelastic scattering and trapping/desorption. The rotational dynamics associated with these two regimes are markedly different. A neat supersonic NO beam is scattered at normal incidence from a Pt(111) crystal at 375–475 K. The non-Boltzmann rotational population distribution of the scattered species exhibits considerable rotational excitation beyond the energy available from the incident beam. Thus, a surface vibration to rotational energy transfer mechanism must be operative. The accompanying rotational alignment data reveal that highly excited rotational states exhibit predominantly "cartwheel" motion. In contrast, rotationally excited molecules that desorb from a 553 K Pt(111) surface show a preference for "helicopter" motion. The opposite preferences for rotational alignment in the two dynamical regimes provide insight into the anisotropy of molecule–surface interactions.

I. INTRODUCTION

Dynamical studies of molecular and atomic scattering on solid surfaces are essential for a complete understanding of the detailed mechanisms of direct inelastic scattering, trapping, and desorption.[1–4] These processes are governed not only by thermodynamics, but by the features of the potential energy surface and the degree of energy transfer in the system. State-selective detection techniques allow the experimentalist to investigate the energy disposal of molecule–surface encounters in a detailed fashion. For the case of molecular scattering, where dissociation and recombination do not play a role, measurement of the rotational population and alignment distributions often provides the most sensitive probe of the dynamics in the system.

The rotational dynamics of several molecule–surface systems have recently been explored using laser detection/molecular beam scattering techniques: NO/Ag(111),[5–12] NO/Cu,[13] NO/Ge(111),[14] NO/GeO_x,[14] NO/graphite,[15–17] NO/Ir(111),[18,19] NO/LiF,[20,21] NO/Ni(111),[22] NO/Pt(111),[23–27] NO/[Pt(111) + O],[24] NO/MgO(100),[28] CO/LiF(100),[29] HF/LiF(100),[30] I_2/LiF(001),[31] NH_3/W(100),[32,33] NH_3/Au(111),[34] OH/Pt(111),[35,36] and N_2/Ag(111).[37–39] Additionally, laser induced fluorescence has been combined with temperature programmed desorption (TPD) to examine the desorption dynamics of NO from Ru(001)[40,41] and Pt(111).[42,43] Together, these studies have investigated the regimes of direct inelastic scattering, indirect inelastic scattering, and trapping/desorption.

The categorization of molecule–surface encounters into one of these three regimes is justifiable in some cases, though this delineation becomes rather difficult for most scattering systems. "Direct inelastic scattering" refers to a single collision between the molecule and the surface in which energy is transferred. "Indirect inelastic scattering" implies that multiple collisions with the surface occurred before the molecule's escape. "Trapping/desorption" involves a relatively long intermediate lifetime on the surface during which equilibration between the surface and trapped molecule occurs.[44,45] In this latter case, the desorbed molecule's final state distribution is characterized solely by the conditions of the surface rather than the molecule's initial conditions. The NO/Ge(111),[14] NO/GeO_x,[14] NO/graphite,[15–17] NO/Ir(111),[18,19] NO/Ni(111),[22] NO/Pt(111),[23–26] NO/[Pt(111) + C],[24] [NO/Pt(111) + O],[24] and NH_3/W(100)[32,33] systems are believed to access all three dynamical regimes over a range of surface temperatures. The inelastic scattering and trapping/desorption channels are distinguished by differences in their respective velocity distributions, surface residence times, and rotational distributions.

In general, the rotational distribution characteristic of direct inelastic scattering is non-Boltzmann. For relatively high beam energies (0.1–1.0 eV, corresponding to 10–100 kJ/mol) a rotational rainbow is commonly observed.[7–11,37–39] A rotational rainbow is a manifestation of a singularity in the differential cross section for rotational excitation. Consider an initially nonrotating ellipse scattering from a flat surface. There will be no translational–rotational energy transfer for collision geometries where the ellipse strikes the surface "end-on" or "side-on." However, all molecular orientations in between these two limits will lead to rotational excitation, with the maximum energy transfer occurring close to 45°. This produces peaks in the rotational distribution both at $J = 0$ and at high J. Luntz, Kleyn, and Auerbach observed a rotational polarization for NO scattering from Ag(111).[9–11] They found that the scattered molecules ($15.5 < J < 35.5$) preferentially rotate in a plane perpendicular to the surface ("cartwheel" motion). Sitz, Kummel, and Zare observed an even stronger polarization for the N_2/Ag(111) system.[37–39] Additionally, Sitz, Kummel, and Zare measured a rotational orientation, i.e., a preference for clockwise vs counter-clockwise rotation, for certain scattering angles.[38]

[a] Current Address: Department of Chemistry, University of Notre Dame, Notre Dame, IN 46556.

 0021-9606/89/173182-14$02.10

The desorption studies have concluded that rotational distributions appear Boltzmann. They are characterized by temperatures which are equal to the surface temperature (for low T_s) or are less than the surface temperature (for high T_s). This phenomenon, termed "rotational cooling," can be understood through the use of detailed balance arguments.[47,48] Desorption is related to adsorption in that one is the inverse of the other. For a system at thermal equilibrium, the desorption rotational temperature will equal the surface temperature only if adsorption occurs for all rotational states, J, with equal probability. If on the other hand, adsorption (and therefore desorption) is hindered for rotational states of high J relative to those of low J, then the desorption rotational temperature will be somewhat lower than the surface temperature.

Jacobs *et al.* reported the only observation of rotationally resolved alignment of molecules desorbing from a single crystal surface.[27] They found that NO, at high J, preferentially desorbs from Pt(111) with its plane of rotation parallel to the surface. Novakoski and McClelland measured for the first time a preferential molecular orientation for the desorption of CHF_3 from Ag(111).[49] Using electric deflection techniques, they observed that CHF_3 tends to desorb with its hydrogen atom oriented toward the surface, while scattering leaves the molecule with a weak orientation in the opposite sense. Utilizing similar techniques, Kuipers *et al.*[50] also found that the incident molecular orientation of NO plays an important role in determining the scattering angular distribution from a Ag(111) surface.

It is the delicate yet consequential regime between inelastic scattering and trapping/desorption that we choose to examine further. Our goal is to better understand the dynamical biasing that distinguishes which molecular configurations lead to trapping and which lead to scattering. Certainly the shape and depth of the molecule–surface potential as well as the coupling of molecular translation and rotation to surface motion will play vital roles in these processes. The measurement of rotational alignment will serve as a probe of both the dynamics and the surface residence time. Our choice of the NO/Pt(111) system is based on a few salient factors. Nitric oxide can be state-selectively detected with very high sensitivity using $1+1$ resonance enhanced multiphoton ionization (REMPI). Moreover, the treatment for reducing $1+1$ REMPI spectra to population and alignment distributions has been developed and tested for the NO system.[51] The Pt(111) surface is the only metal substrate on which the NO molecule has a large binding energy (25–35.5 kcal/mol, corresponding to 105–149 kJ/mol) and yet does not appreciably dissociate.

The interactions between NO and Pt(111) have been studied previously using a number of complementary techniques. These have evaluated molecule–surface binding energies, core level shifts, vibrational frequencies, long-range order, sticking probabilities, and accommodation coefficients for a variety of surface temperatures and coverages.

The thermal desorption data[52–55] indicate that there are at least three distinct temperature peaks at which NO molecularly desorbs from a Pt(111) surface. These occur at 190, 320, and 375 K. The high temperature peak is assigned to a bridge site[53,55,56] with a binding energy of 35.5 kcal/mol (149 kJ/mol).[54] The bridge site refers to an equilibrium geometry where the NO binds to two neighboring Pt atoms. It has a characteristic vibrational spectrum, measured both by electron energy loss (EELS)[53,57] and infrared absorption spectroscopy (IRAS),[55] and produces a shift in the N($1s$) and O($1s$) core levels, as detected by XPS.[56] These techniques have also determined that the 320 K desorption peak contains both bridge-bonded and atop species.[53,56] Atop defines the geometry where the NO molecule binds to a single Pt atom in a linear arrangement. The electron impact behavior suggests that the NO is bound through the nitrogen atom,[52] consistent with organometallic analogs.[58,59] At low coverage, the bridge site fills preferentially. The atop site is occupied at higher coverage and forms a $p(2\times2)$ structure, as seen by low-energy electron diffraction (LEED).[53,55–57] This structure saturates at 0.25 monolayers and thus continued adsorption proceeds to fill weakly bound (190 K thermal desorption peak) disordered sites within the $p(2\times2)$ structure.

The fraction of nitric oxide which decomposes on the Pt(111) face is less than 2%.[54,60] The small amount of dissociation that does take place occurs at the minority defect sites.[53] These defect sites are quickly blocked from further reactivity by tightly bound atomic oxygen.

Molecular beam studies of NO on Pt(111) have revealed that the initial sticking probability, i.e., the probability of a gas-phase molecule binding to the surface at low surface coverage, is large (0.65[61]–0.9[60,62]) and rather insensitive to surface temperature.[60,62] The sticking probability varies nonlinearly with coverage, suggestive of an extrinsic precursor state.[62] The desorption kinetics have been well described by a model[63] which takes into account the role of step (defect sites) and terraces [regions exposing only the (111) plane]. The rate limiting step for desorption at low coverage appears to be diffusion from the steps to the terraces. On the terrace, the NO molecule desorbs with a much higher probability.[63,64]

The angular and velocity distributions of NO scattered from Pt(111) indicate the coexistence of inelastic scattering and trapping/desorption channels, with the latter being predominant.[65] The translational energy accommodation factor is near unity for surface temperatures less than 900 K. At higher surface temperatures, the translational temperature of the scattered species falls below the surface temperature. A similar effect is seen for both the vibrational and rotational degrees of freedom; however, the deviations from unity are more dramatic and occur at lower surface temperatures.[23–26,42,43] The spin–orbit temperature was found to be identical to the measured rotational temperature.[41] The two Λ doublets within each spin–orbit state were observed to have equal populations.[41] The Λ-doublet states, in the high J limit, are distinguished by the direction of the partially occupied $2p\pi$ orbital relative to the plane of rotation.

It appears from this summary that NO equilibrates rapidly and efficiently with the Pt(111) surface, that adsorption is nonactivated, and that product distributions should exhibit purely statistical behavior, i.e., no dynamical biasing. However, examination of the directional anisotropy of the

scattered molecule's rotational angular momentum reveals much more about the dynamics of inelastic scattering, trapping, and desorption.

II. EXPERIMENTAL

The experiment utilizes a UHV scattering chamber, a tunable UV laser source, and a variety of support electronics. A Varian UHV surface analysis chamber is adapted to support a pulsed molecular beam source and state-selective detection (see Fig. 1). The main chamber houses a sample manipulator which allows X,Y,Z translation, rotation of the 2.5 in. offset sample arm about the center axis of the chamber, surface tilt rotation, and surface temperature control through a combination of radiative and electron bombardment heating as well as liquid nitrogen cooling. Heating of the surface is controlled by a feedback circuit in order to keep the surface temperature constant to within 1 K throughout a wavelength scan. The chamber is equipped with LEED and Auger electron spectroscopy (AES) diagnostics, a quadrupole mass spectrometer, and an Ar^+ sputtering gun for surface analysis and preparation. Additionally, the apparatus includes a quartz window to permit entry of the excitation laser light and a time-of-flight (TOF) ion drift tube for ion mass separation and collection. Ions are produced by $1+1$ resonance enhanced multiphoton ionization (REMPI). The time-of-flight mass selection allows for discrimination against nonresonant ionization of background impurities. The tube's custom design consists of an extraction grid, an acceleration grid, steering plates, a 30 cm drift tube, and a channel electron multiplier array (CEMA) (Galileo Optics FTD 2002). The main chamber is pumped by a 220 ℓ/s ion pump, a titanium sublimation pump, a liquid nitrogen cryopanel (all from Varian), and a 1500 ℓ/s turbo-

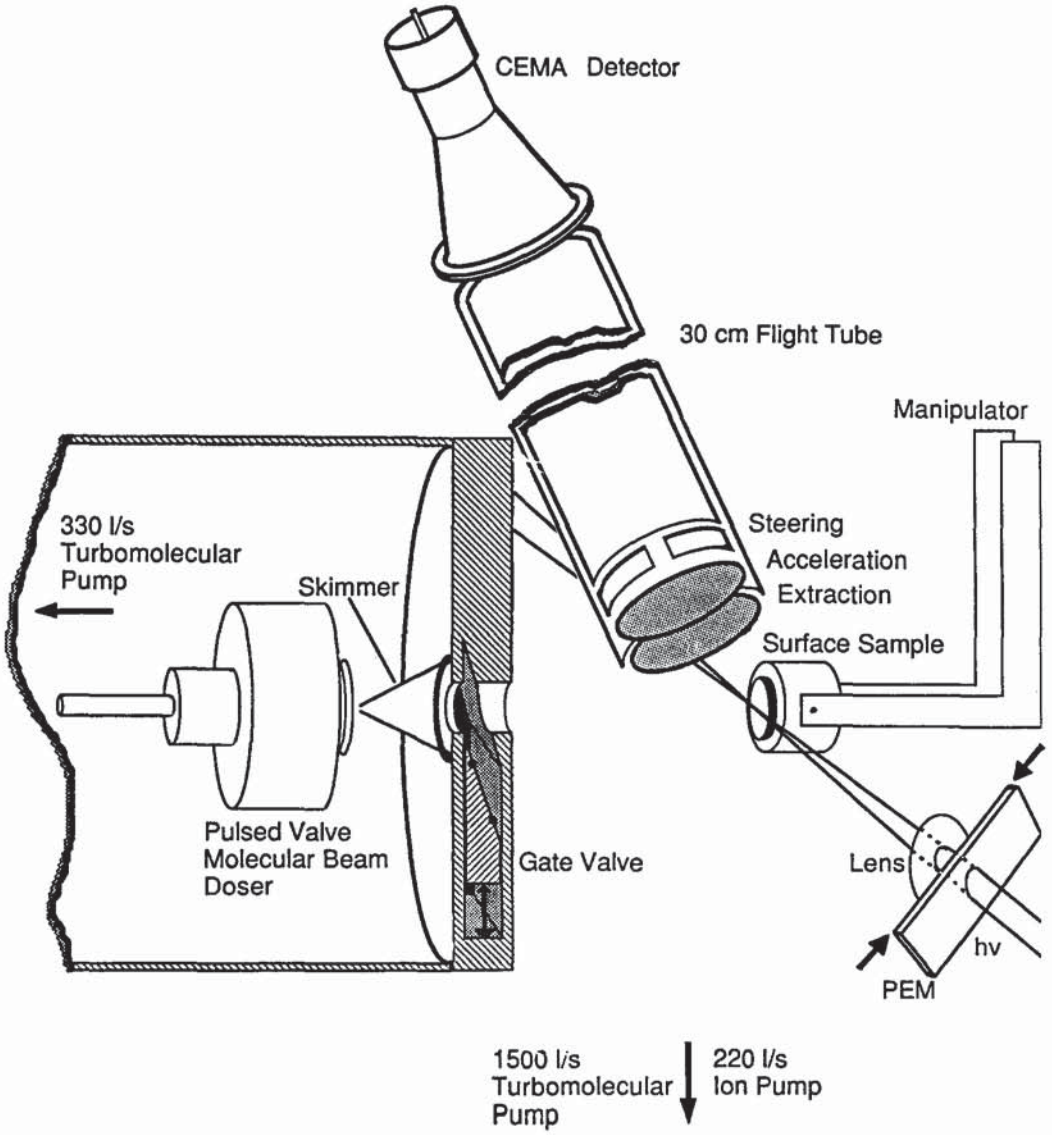

FIG. 1. Experimental apparatus. A differentially pumped pulsed valve doses the Pt(111) crystal. Laser radiation is focused 2 mm above the surface. Ions produced in the REMPI process are accelerated through the time-of-flight tube and collected by the CEMA. The crystal can be rotated in order to face LEED and AES diagnostics. Not shown are Helmholtz coils which cancel the earth's magnetic field and leave a residual magnetic field in the direction of the surface normal.

molecular pump (Balzers) which allows us to maintain a base pressure of 3×10^{-10} Torr during the experiment.

An invaginated source chamber is attached to one of the main chamber's standard 8 in. conflat flanges. The 3/4 in. thick flange separating the two chambers contains a motorized gate valve. This valve permits either chamber to be vented to atmosphere without affecting the pressure of the other chamber. A Lasertechnics pulsed valve, with a 0.1 mm nozzle orifice, is mounted kinematically to this interfacial flange. The supersonic beam is collimated with a 0.3 mm skimmer so that the beam strikes only a 5 mm diameter region of the surface. The 10 cm nozzle–surface distance allows instantaneous pulsed molecular beam fluxes as high as 10^{17} molecules/(cm^2 s). The source chamber is pumped by a 330 ℓ/s turbomolecular pump (Balzers).

The generation of tunable ultraviolet laser radiation relies on a commercial 10 Hz Quantel 581C Datachrom System. The frequency doubled Nd:YAG laser pumps a Moya oscillator cavity dye laser (0.08 cm^{-1} bandwidth). This tunable output is frequency doubled and Raman shifted (second order anti-Stokes) in H_2. The resulting Raman orders are separated with matched 60° quartz prisms. This system creates 6 ns pulses at 224 nm with approximately 200 μJ of energy per pulse. A 5 mm diameter homogeneous spatial region of the radiation is selected, via an iris diaphragm, to be focused into the chamber. On each laser shot the computer selects the direction of the laser light's plane of polarization via a photoelastic modulator (PEM). The PEM eliminates beam walk associated with other polarization rotators and produces light which is greater than 99.5% linearly polarized. A back-reflection of the 224 nm light is focused onto a pyroelectric detector for shot-to-shot monitoring of the laser energy. The remainder of the radiation passes 2 mm above the surface as it propagates parallel to the Pt crystal face. A 25 cm focal length lens is used to focus the light 5 cm before it reaches the ionization region above the surface. In this region the beam diameter is approximately 0.5 mm. This focusing geometry reduces the level of saturation in the REMPI process.[51]

Due to the $^2\Pi$ symmetry of the NO ground state, stray magnetic fields can scramble the rotational alignment of the product distribution during the molecule's 1 μs flight time from the surface to the laser ionization region. In order to minimize stray magnetic fields,[66] Helmholtz coils are installed around the exterior of the main chamber. Symmetric pairs of electromagnetic coils are placed along the X, Y, and Z directions of the apparatus. The regulated currents flowing through these coils are adjusted so that a small field, pointing along the surface normal, remains in the ionization region.[67] In addition, the filament current used to heat the surface is turned off for 10 ms during the laser pulse.

The ion signal and the laser energy, as measured by the pyroelectric detector, are digitized with a CAMAC LeCroy charge sensitive gated integrator and stored on a DEC PDP 11/23 computer. The ion signal is normalized to the square of the pyroelectric sector output on a shot-by-shot basis. The computer also controls the laser wavelength, polarization direction, surface temperature, and delay between the pulsed nozzle and the firing of the laser.

All experiments reported here are performed with a 50 psi neat expansion of NO gas (99% rated purity[68]) at normal incidence to the Pt(111) surface. The measured rotational temperature of the beam is 40 K.[69] Under similar expansion conditions, Serri, Cardillo, and Becker[60] found the translational energy of a neat NO supersonic beam to be 9.2 kJ/mol. The ratio of dimers to monomers in the beam is estimated to lie between 10^{-3} [70] and 10^{-2}.[60] The pulsed molecular valve delivers gas pulses as short as 90 μs FWHM.

Two different Pt(111) crystals were used during this investigation. *No difference in rotational distributions was observed between the two crystals.* Both were cut from a 1 cm boule of 99.999% single-crystal platinum. The first surface was aligned to within 1.5° of the (111) face; the second to within 0.5°. Both crystals were polished with diamond pastes down to a final grit size of 0.5 μm. Final polishing was done with 0.005 μm alumina. The surface is cleaned by annealing at 900 °C in the presence of approximately 10^{-8} Torr of O_2 and flash desorbing the resulting oxide at 1200 °C. AES is employed to determine surface cleanliness. Treatments are repeated until impurity levels reach the noise level of our Auger spectrometer (approximately 1%–2% of a monolayer). Between experimental runs the crystal is annealed for one minute at 800 °C. AES is also performed at the end of a set of experimental runs. It was found that O was the only impurity to build up (see below).

During the experiment, the surface quickly reaches a steady-state coverage of molecular and dissociated NO.[62–64] The atomic species are believed to originate from dissociation at defect sites on the surface. Because of the greater binding energies for atomic oxygen at defect sites, adsorbed oxygen blocks these sites from further reactivity. Thus, the concentration of atomic oxygen saturates at a level approximately equal to the concentration of defect sites, which we believe from our AES results to be $<5\%$.

The dynamical regimes of direct inelastic scattering and trapping/desorption are differentiated according to their characteristic surface residence times. The residence time for direct inelastic scattering is infinitesimal compared to the microsecond time scale of the molecular beam pulse. However, the trapped state will exhibit a half-life on the surface which is inversely proportional to the desorption rate constant. For our temperature regime, the half-life is estimated to be 2–2000 ms. Figure 2 illustrates the calculated surface temperature dependence of both the steady-state coverage and the surface residence time for a range of incident molecular fluxes. For the calculation, we utilized the coverage-dependent preexponential factors and activation energies for desorption determined by Campbell, Ertl, and Segner.[62]

A 100 μs nozzle pulse at a 1×10^{17} molecules/cm^2 s peak flux delivers 0.006 Langmuirs to the surface and creates a pressure rise in the main chamber of $<1\times10^{-10}$ Torr. Hence the instantaneous coverage during the nozzle pulse will only be slightly higher than the steady state coverages reported in Fig. 2.

Numerical integration of the rate equations for adsorption and desorption yields a prediction of the total and fractional components of the scattered temporal waveform (see Fig. 3). Here we again use the coverage-dependent sticking

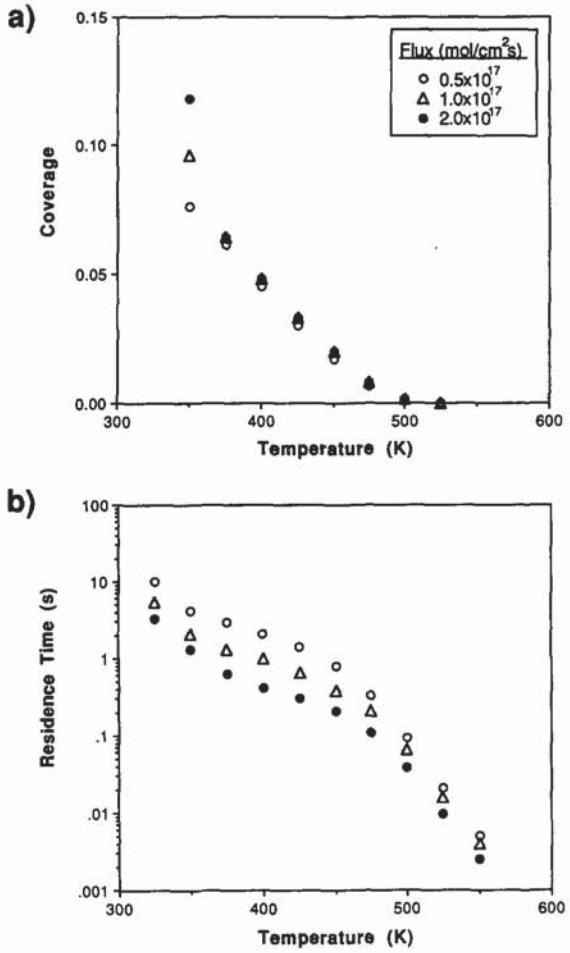

FIG. 2. Temperature dependence of the (a) steady-state coverage and (b) surface residence time for NO on Pt(111). Calculations are performed for three values of the instantaneous molecular beam flux.

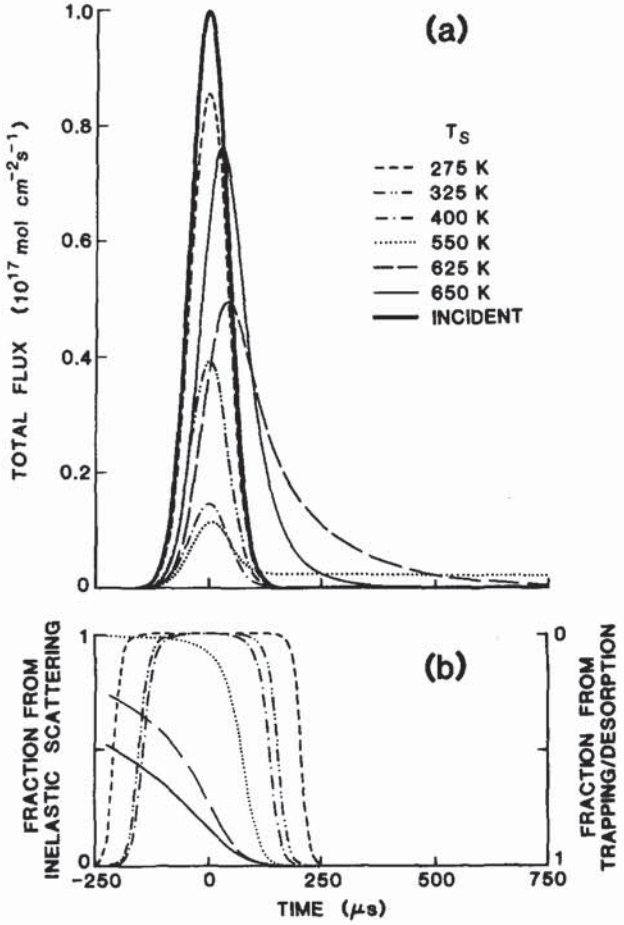

FIG. 3. (a) Total and (b) fractional (inelastic scattering vs trapping/desorption) components for the scattered flux of NO from Pt(111) at various surface temperatures. Calculations approximate an incident molecular beam pulse with a Gaussian function [1×10^{17} mol/(cm^2 s) instantaneous flux, 100 μs FWHM].

probability and desorption rate constants determined by Campbell, Ertl, and Segner.[62] Figure 3(a) shows the incident Gaussian waveform and the calculated scattering waveforms for a range of surface temperatures. Conservation of mass requires the integrated intensity of each of these profiles (over the 100 ms delay period) to be equal to the integrated flux incident on the surface. Figure 3(b) illustrates the fraction of scattered intensity that is associated with inelastic scattering and conversely trapping/desorption channels. The calculated flux emanating from the surface is integrated over all detection angles. Hence the contribution of inelastically scattered flux may be underestimated for normal incidence/normal detection geometries. At low surface temperatures ($190^{71} < T_s < 300$ K), the surface coverage approaches saturation and the sticking probability converges to zero, while the trapping probability remains near unity.[60,72] The resulting scattered waveform then approximates the incident waveform, where the majority of the intensity is attributed to trapping/desorption in a short-lived extrinsic precursor on the NO-covered surface. At moderate surface temperatures ($300 < T_s < 525$ K), the surface coverage remains low and the scattered profile resembles an attenuated version of the incident pulse. The attenuation is related to the effective sticking probability at the steady-state coverage. Desorption takes place on a relatively long timescale and does not contribute to the flux leaving the surface during the molecular beam pulse. At relatively high temperatures ($T_s > 525$ K), desorption occurs on a timescale comparable to the incident pulse. However, the desorption decay is visible only for a narrow range of temperatures (525–650 K). Beyond 650 K the scattered profile again resembles the incident waveform, although the fraction of inelastic scattering during the molecular beam pulse is only 10%, or one minus the initial sticking probability.

Figure 3 demonstrates that there are narrow windows in temperature and coverage for which these experiments can probe the distinct processes of inelastic scattering and trapping/desorption. Specifically, inelastic scattering from clean Pt(111) is uniquely accessed for surface temperatures ranging from 400 to 525 K. Below 400 K the steady-state molecular NO surface coverage might begin to interfere with the scattering dynamics. Above 525 K, trapping/desorption starts occurring during the molecular beam pulse, thus dilut-

ing the inelastically scattered component. The regime of trapping/desorption must be probed after the completion of the molecular beam pulse. Consequently, desorption measurements can only be performed at surface temperatures between 550 and 650 K. Beyond this narrow range there is little or no intensity for state-selective detection of desorbates. This temperature range also constrains these desorption studies to operate in the very low coverage limit ($<0.1\%$ of a monolayer). Of course, these kinetic calculations are approximate, but our measured alignment distributions confirm the basic principle of temporal discrimination.

III. ANALYSIS

Experimentally, we observe quantities that pertain to the molecule's total angular momentum vector **J**. The total angular momentum is composed of nuclear rotation N, orbital angular momentum L, and electron spin S. This study observes both the relative population and degree of rotational alignment in each quantum level J. Relative population refers to the fraction of molecules in the level J, and rotational alignment is a measure of the anisotropy in the spatial distribution of the vector **J**. Rotational alignment is conveniently described by the even moments of the total angular momentum distribution. In cases of cylindrical symmetry, $1+1$ REMPI through the NO A–$X(0,0)$ band will only be sensitive to the population and the quadrupole moment, $A_0^{(2)}$.[51,66]

Classically, the quadrupole moment is defined to be twice the expectation value of the second order Legendre polynomial with respect to the projection of the angular momentum vector **J** on the cylindrical symmetry axis. It is a measurable quantity, whose value spans from $+2$ to -1,[73] where these limits correspond to the molecule rotating in a plane parallel to the surface ("helicopter" motion) or in a plane perpendicular to the surface (cartwheel motion), respectively (see Fig. 4). A quadrupole moment of zero suggests no preferential alignment of rotation.

The recorded REMPI spectra must be properly analyzed to extract accurate relative populations and alignment factors.[51,66] A theoretical treatment has been developed for reducing $1+1$ REMPI spectra to rotational state distributions.[66] Additionally a methodology has been formulated for both data collection and analysis phases.[51] We include here the specific formulas required for analyzing data recorded under one commonly employed polarization scheme.

The ionization transition in $1+1$ REMPI through the $v=0$ level of the $A\,^2\Sigma^+$ state in NO has been characterized previously.[51] The cross section for ionization was found to have a relatively mild dependence on the intermediate state alignment.[74] Consequently, the $1+1$ REMPI scheme is only sensitive to the population and quadrupole alignment moment of NO.[75] This result simplifies the extraction of alignment information in that the ion signal need only be measured for two independent planes of linearly polarized light.

In the lab, we record spectra under conditions where the polarization direction of the laser is either parallel or perpendicular to the surface normal. This is performed by alternating the polarization between these two directions throughout the entire wavelength scan. For a given rotational transition out of a rotational state J, we identify $I_\parallel$ and $I_\perp$ as the integrated ion intensities for which the laser polarization is parallel or perpendicular to the surface normal (the cylindrical symmetry axis). The relative population $N(J)$ and the quadrupole alignment moment $A_0^{(2)}(J)$ are related to these measured intensities by

$$N(J)=\frac{I_\parallel+2I_\perp}{\Sigma_M F_{\rm sat}[k_{01}(M),k_{12}(M),I\Delta t]}, \tag{1}$$

and

$$A_0^{(2)}(J)=\frac{2\{I_\parallel-I_\perp\}\Sigma_M F_{\rm sat}[k_{01}(M),k_{12}(M),I\Delta t]}{\{I_\parallel+2I_\perp\}\Sigma_M\{3[M^2/J(J+1)]-1\}F_{\rm sat}[k_{01}(M),k_{12}(M),I\Delta t]}, \tag{2}$$

where M is the quantum number representing the projection of **J** on the cylindrical symmetry axis, $k_{01}(M)$ is the M-dependent transition probability for the resonant photon step, $k_{12}(M)$ is the M-dependent transition probability for the ionization step, $I\Delta t$ is the measured laser fluence, and $F_{\rm sat}$ is a function which calculates the overall $1+1$ REMPI ionization probability while including the effects of saturation and intermediate state alignment. The analytical form of $F_{\rm sat}$, as well as $k_{01}(M)$ and $k_{12}(M)$, have been worked out previously.[51,66]

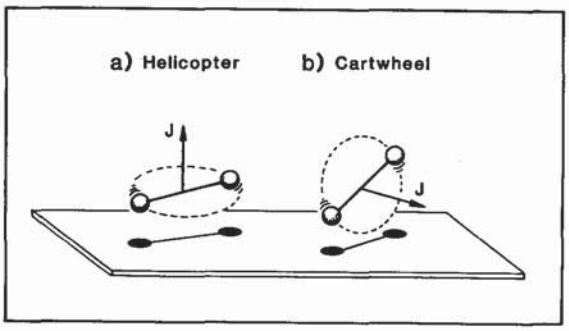

FIG. 4. Rotational alignment relative to the surface plane. The helicopter motion (a) is favored for $A_0^{(2)}>0$ while the cartwheel motion (b) is favored for $A_0^{(2)}<0$,

IV. RESULTS

A. Inelastic scattering

The dynamical regime of inelastic scattering is selectively explored by firing the laser synchronously with the rising

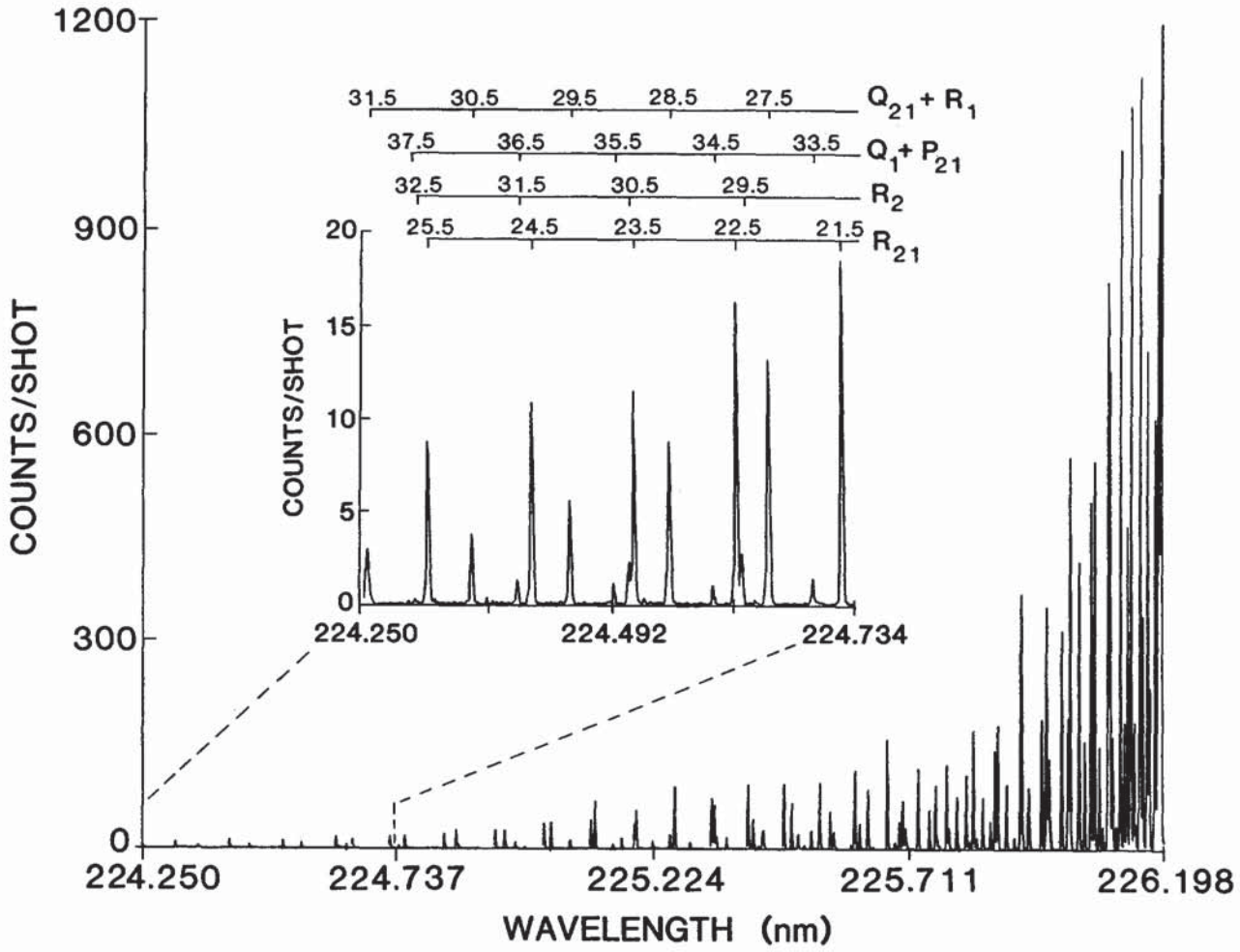

FIG. 5. Spectrum of NO scattering from a Pt(111) surface at 400 K. The inset provides an expanded view of the high J region. The rotational transitions of the resonant excitation step are assigned.

edge of the nozzle gas pulse.[76] The laser is scanned at a rate that permits, for each rotational line profile, approximately 50 laser shots of signal averaging for each of the two orthogonal laser polarizations. Scattering of the neat supersonic beam is studied at five different surface temperatures, selected between 375 and 475 K. These temperatures exceed the molecular beam formation temperature (298 K), i.e., the temperature of the beam if the initial energy in the molecule were evenly divided among all degrees of freedom. These initial conditions favor surface vibrational to molecular energy transfer.

A typical spectrum of NO scattered from a 400 K Pt(111) surface is shown in Fig. 5. This section of the spectrum contains predominantly branches arising from the $^2\Pi_{1/2}$ ground spin–orbit state. A portion of the figure is expanded to illustrate the signal to background ratio that is routinely realized with $1+1$ REMPI. Our dynamical range for extracting populations is on the order of 12 natural logarithm units, or $>10^5$.

The spectra, recorded at orthogonal laser polarizations, are reduced to the Boltzmann rotational population plots shown in Fig. 6. Here we plot the natural logarithm of the population (divided by its degeneracy and compensated for saturation and intermediate state alignment) vs the rotational energy. This plot would yield a straight line if the data were described by a Boltzmann distribution. The data points clearly deviate from a linear form. It has been found that submonolayer coverages of C have little effect on the rotational distribution compared to clean surface results.

The relatively large population at low J is attributed to detection of the incident molecular beam.[76] Although this interferes with the population analysis for $J<7.5$, it provides a convenient means of normalization for the various data sets. We assume that the predominant contribution to the population observed at $J=0.5$ comes from the incident beam. Hence, scaling the plots so that they intersect at $J=0.5$ effectively normalizes the data to constant beam flux.

The dashed vertical line at 690 cm^{-1} represents the total energy in the incident molecular beam. In the rigid surface limit, rotational excitation beyond this energy would be strictly forbidden.[77] However, the present experiment demonstrates that a considerable fraction of the scattered molecules contains more rotational energy than imposed by this limit. In fact, the amount of rotational excitation in the scattered distribution increases with increasing surface tempera-

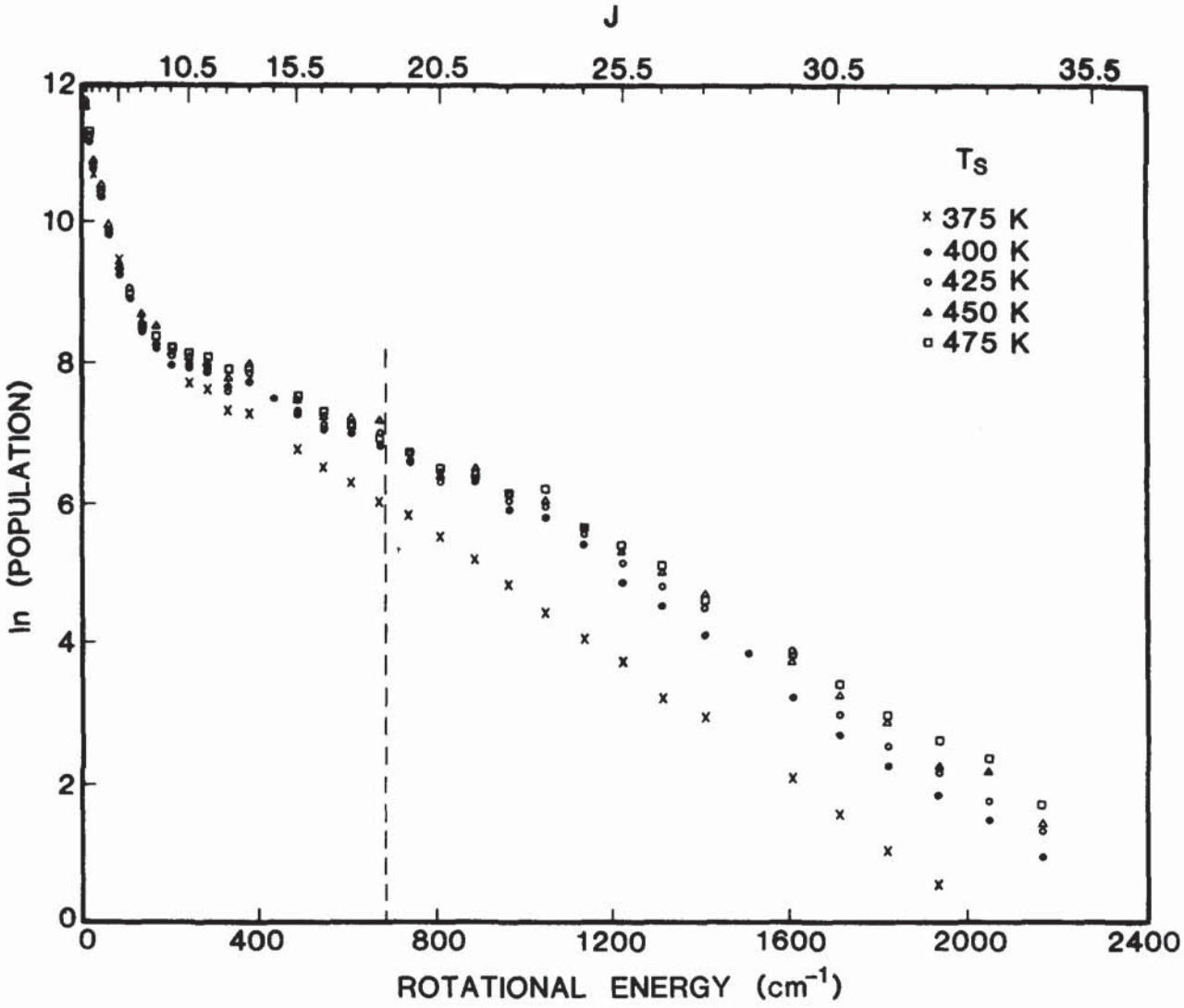

FIG. 6. Boltzmann plot of the rotational distributions for NO scattered from Pt(111). The temperature of the surface is indicated for each set of data. The data are normalized to the populations in $J = 0.5$. The dashed vertical line represents the total energy in the incident beam.

ture. This is most easily seen in the deviations of the relative populations in the highest rotational states as recorded for different surface temperatures.

Figure 7 shows the accompanying quadrupole alignment moment for the scattered molecules versus their rotational quantum number J. For $J < 10.5$ there is no appreciable alignment. Of course, interference by the incident beam as well as hyperfine depolarization will dilute the amount of observable alignment in this region. Beyond $J = 10.5$ there is a steady rise in the rotational alignment until it peaks around $J = 25.5$. The maximum alignment observed corresponds to a quadrupole moment of -0.5. Recall that $A_0^{(2)}$ has a limiting value of -1, which occurs when all the molecules rotate with a cartwheel-type motion. For $J > 25.5$, the alignment again decreases. The alignment measured at the highest J values has an uncertainty of ± 0.2 caused by the low signal intensity.

For clarity, Figs. 6 and 7 include only the population and quadrupole moment values measured for the $^2\Pi_{1/2}(A'')$ state. Here, the A'' notation refers to the symmetry of one of the two Λ doublets.[78] In the high J limit, the unpaired electron of the A'' Λ doublet has a higher probability of lying along J than in the plane of rotation. We found that both Λ doublets contained equal populations (within 10%), as reported previously.[43] The alignment measurement for the A' state of the $^2\Pi_{1/2}$ level is difficult because of congestion in one branch and branch mixing in the other. However, the two Λ doublets of opposite symmetry in the $^2\Pi_{3/2}$ state exhibit similar rotational population and alignment distributions.[43,79]

B. Trapping/desorption

The desorption channel is isolated by firing the laser 200 μs after the completion of the nozzle pulse,[80] thus eliminating contributions from inelastic scattering channels. The molecular beam then serves as a reproducible pulsed doser for the system. Because of the low signal levels in this operating regime, accurate alignment moments cannot be extract-

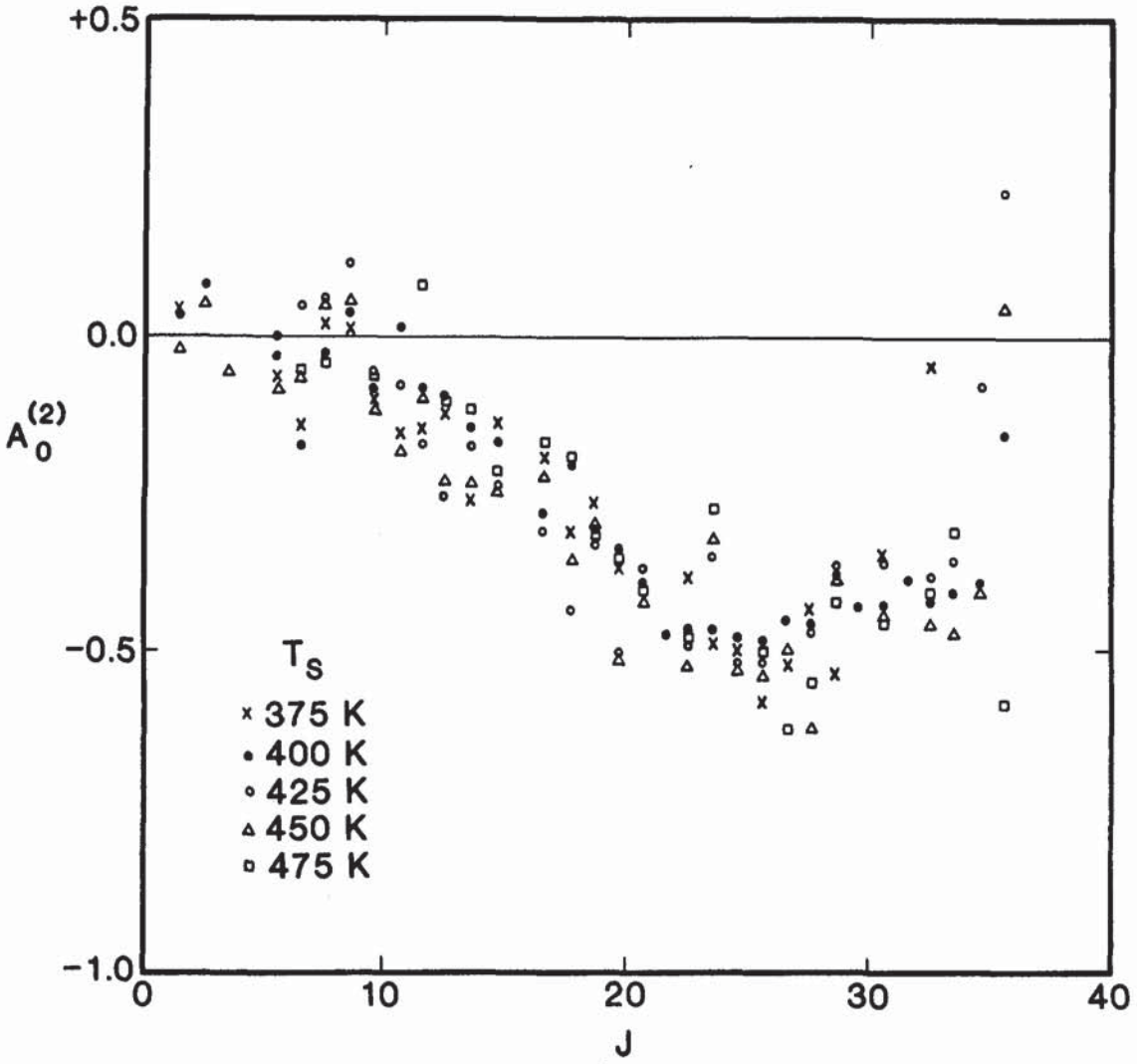

FIG. 7. Quadrupole moment alignment distribution as a function of the rotational quantum number J is plotted for the case of inelastic scattering of NO from Pt(111). The surface temperatures at which each set of data was recorded are indicated.

ed during the course of a wavelength scan. Therefore, the laser is tuned to a specific rotational transition and ions are collected for 1000–10 000 laser shots at alternating laser polarization directions. The measured intensities are analyzed using Eq. (2). The alignment distribution for desorption is measured only at $T_s = 553$ K because, within the limited temperature range in which desorption predominates, lower surface temperatures do not produce sufficient desorption flux and higher surface temperatures introduce some hot-band congestion in the high-J region of the (0,0) band.

Figure 8 shows the quadrupole moment, $A_0^{(2)}(J)$, as measured from two different rotational branches of the same $^2\Pi_{1/2}$ Λ-doublet state. There is little to no rotational alignment for $J < 12.5$, while higher rotational levels show increasing values of the quadrupole moment. A positive quadrupole moment indicates a preference for rotational motion similar to that of a helicopter (see Fig. 4). As in the case of direct inelastic scattering, the Λ-doublet states in both spin–orbit levels exhibited similar degrees of alignment.

Rotational populations are found to match those of previous results[23–26] and are, therefore, not reported here.

V. DISCUSSION

These experiments cover new ground in the field of gas–surface dynamics. They represent the first observation of rotational alignment in molecular desorption. Additionally, this marks the first study of inelastic scattering in which rotational levels up to three times more energetic than the incident beam energy are examined for rotational alignment. Although significant surface to rotational energy transfer is responsible for populating states with rotational energy exceeding the beam energy, rotational alignment is created in these states and is preserved in the final distribution. The observation of opposite preferences for rotational alignment in desorption and inelastic scattering further exemplifies the interesting dynamics at work in this chemical system.

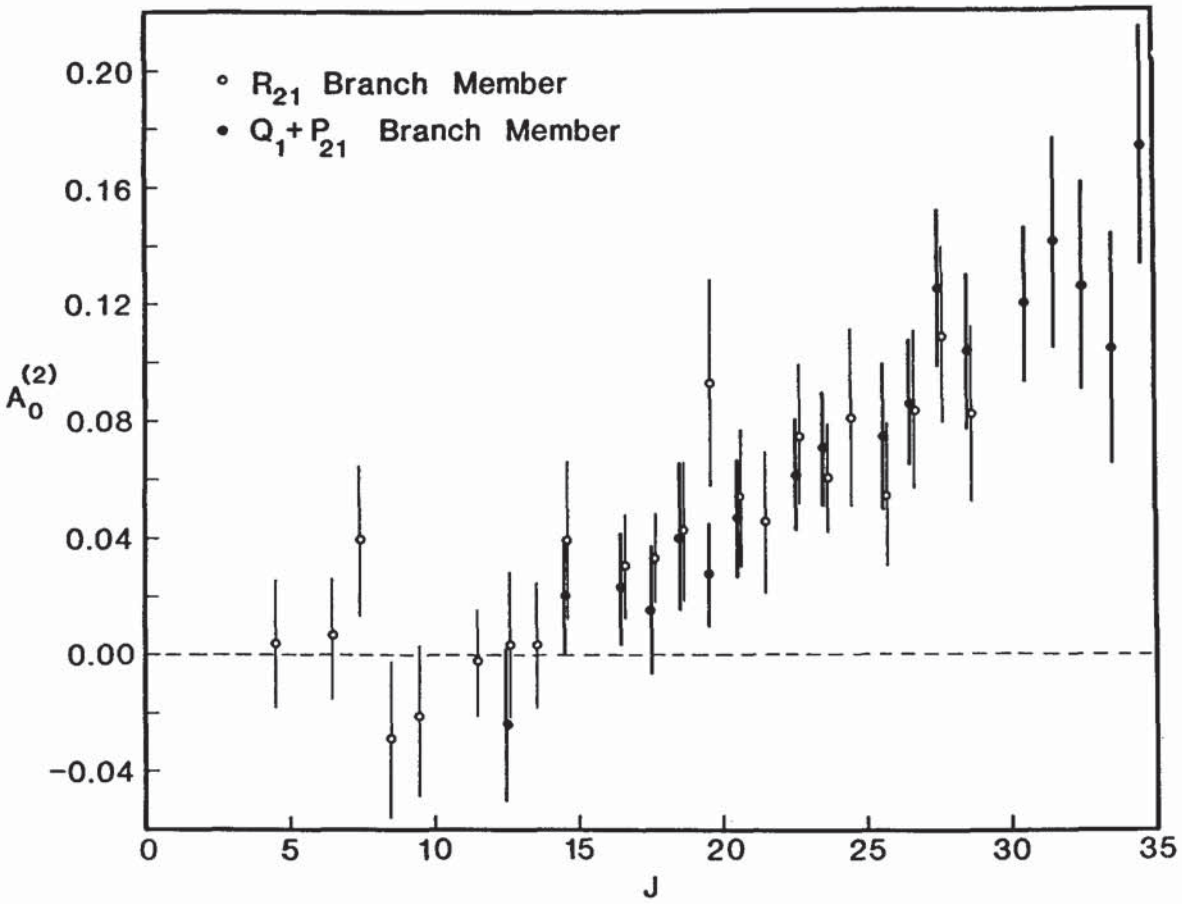

FIG. 8. Quadrupole moment alignment distribution for NO desorption is plotted against rotational quantum number J. The Pt(111) surface temperature is 553 K.

A. Rotational populations

The Boltzmann plots of Fig. 6 show the results for inelastic scattering of NO on Pt(111) at surface temperatures of 375–475 K. Rotational population decreases monotonically with increasing J, and the scattering populates rotational levels with energies exceeding the total incident beam energy. Excluding the low J interference, one might like to describe the inelastic scattering population distributions (for $400 \leqslant T_s \leqslant 475$ K) as Boltzmann and consider the scattered NO to be thermally accommodated. In fact, the scattered distributions are not well described by a single line, but instead exhibit a positive curvature. A bimodal distribution is only associated with negative curvature, and can therefore be excluded. In contrast, the direct inelastic scattering experiments of NO[7–11] and N_2[37–39] on Ag(111) have attributed positive curvature in the population distribution to the occurrence of a rotational rainbow. In these cases, the rainbow always occurs at a rotational energy below the incident beam energy. The NO/Pt(111) results might combine an orientational singularity in the rotational excitation probability (operative in classical rotational rainbows) with a surface vibrational energy transfer mechanism (leading to a positive net transfer of energy from the surface to the molecule). NO has a large adsorption energy on Pt(111) which serves to accelerate the molecule into the surface and intensify the impulsive part of the scattering collision. Additionally, the polar potential of NO on Pt(111), favoring bonding through the nitrogen atom, contributes to the large degree of rotational excitation.

We have observed that a significant fraction of the inelastically scattered molecules acquires more rotational energy than the molecules initially had available as total energy in the incident beam. Such a phenomenon was also observed in the direct inelastic scattering of NO from Ag(111).[6] Because the incident beam has a narrow velocity distribution and a cold internal state distribution, this energy gain can only come from the surface. Calculations suggest that electron–hole pair transitions in the metal do not contribute significantly to rotational and translational energy transfer.[81,82] Therefore, the most likely mode of energy transfer is through surface vibrations.

We believe a proper description involves the positions and momenta of the surface atoms which interact locally with the molecule, rather than a delocalized phonon-mediated energy transfer mechanism. The latter is thought to be inadequate to explain this energy transfer process because the scattering NO molecule applies a significant perturbation to the surface phonon distribution arising from (i) the strength of the chemisorption potential, (ii) the mass of the

NO molecule, and (iii) the localized nature of the interaction. Classically, if all the energy of one vibrational mode of a surface atom were gained by an NO molecule, it would on average transfer $kT(\sim 300\ \mathrm{cm}^{-1}$ under our experimental conditions). On the other hand, Fig. 6 indicates that some molecules gain as much as 1500 cm^{-1} above the incident beam energy in rotational energy alone. We believe that it is difficult to rationalize this amount of energy transfer by a multiphonon annihilation. The large energy transfer, therefore, suggests the importance of multiple bounces in the inelastic scattering process for those molecules excited to high rotational levels. The latter effect is examined in greater detail in the accompanying paper.[83]

Figure 6 also illustrates that population in any given rotational level changes by less than a factor of 2 as the surface temperature increases from 400 to 475 K. However, there appears to be a dramatic loss in both the rotational excitation probability and scattered intensity of NO molecules striking the 375 K Pt(111) surface. Trajectory calculations of NO scattering from a clean Pt(111) surface do not predict this pronounced behavior.[83] It is possible that scattering occurs on a partially NO covered Pt(111) surface at this temperature, as suggested in Fig. 2(a). This would lead to a greater percentage of out-of-plane scattering and could significantly decrease both the rotational excitation probability and the observed scattered intensity.

B. Rotational alignment

Both inelastic scattering and trapping/desorption regimes yield little rotational alignment for the levels $J < 12.5$, while higher rotational levels show a preferential alignment in both cases. In the case of desorption the alignment distribution implies a preference for helicopter motion, while the inelastic scattering process produces an alignment distribution which is indicative of cartwheel motion. One way to better understand these results is to analyze them in light of the principle of detailed balance.

The principle of detailed balance is a useful guide in the analysis of surface scattering and desorption data. This principle states that for a system at equilibrium, the rates of all forward reactions must exactly balance the rates of all reverse reactions. Thus by observing a given reaction, we are able to invoke this principle and infer information on the process which appears to be its inverse. In one of the earliest applications of detailed balance as it relates to the angular distributions of scattered particles, Clausing[84] has shown that for the case of a gas interacting with a surface at thermal equilibrium, the angular distribution of particles which depart from the surface must follow a cosine flux distribution *when summed over all channels.* Any deviations from this behavior are in violation of the second law of thermodynamics. This problem has been treated more recently by Wenaas[85] who has proved the same conclusion by invoking the closely related principle of reciprocity.[86] A rigorous proof of whether these relations hold for a system far from equilibrium, such as the case of a supersonic jet interacting with a surface of arbitrary temperature, is not available. However, experimental results[87,88] have shown that deviations from the predictions of detailed balance are small.

The case of rotational alignment has not been specifically treated insofar as its relation to detailed balance. However, an extension of the arguments of Wenaas leads to the conclusion that rotational population and alignment distributions should demonstrate reciprocity, i.e., follow detailed balance. Therefore, we can state that for a system at equilibrium we would expect an isotropic flux distribution of angular momenta for those particles departing from the surface *when summed over all channels.* We can state nothing, however, about the distributions of the individual channels, *a priori*, on the basis of detailed balance. As is the common practice, detailed balance is applied not only to the total distribution, but to the direct inelastic scattering channel and the trapping/desorption channel separately.[89]

Consequently, a deeper understanding of the alignment behavior for these two scattering regimes requires a more thorough analysis of how these two processes occur. For this purpose, we have developed a simplified classical trajectory model and applied it to this system. The details and results of the model are reported in the accompanying paper.[83] Interpretation of the experimental data reported here is greatly enhanced by comparison with the predictions of the model. The results of this comparison will be discussed at length in the accompanying paper.[83] However, it is useful at this point to comment on some aspects of the data.

The quadrupole moment, measured for the case of inelastic scattering, shows the expected preference toward cartwheel motion as seen for NO/Ag(111)[9–11] and N_2/Ag(111).[37–39] The preference for cartwheel motion in inelastic scattering arises from molecule–surface forces which lie normal to the surface. The observed quadrupole moment exhibits approximately the same J-dependence for all five surface temperatures and peaks at a value of -0.5.

There are four possible reasons why the quadrupole moment might not reach its limiting value of -1. First, corrugation in the surface potential introduces tangential forces that are not present on a flat surface. Hence, on a corrugated surface the molecule can receive torques which induce rotational motion in a plane other than the pure cartwheel limit predicted for a flat surface. Second, multiple bounces on the surface will tend to scramble alignment, as demonstrated by the trajectory model presented in the accompanying paper.[83] This effect potentially differentiates direct inelastic scattering from indirect inelastic scattering. Third, the low populations in the highest rotational levels are susceptible to a weak but nonnegligible contribution from trapping/desorption. This contribution would most likely have the opposite sense of alignment (as seen in the desorption results reported here), and thus affect the observed alignment more dramatically. Fourth, breaking cylindrical symmetry in the system introduces new nonvanishing moments to the measured alignment distribution. The consequence of this effect is that measurement is made of the "apparent" quadrupole moment rather than the true quadrupole moment.

The apparent quadrupole moment is composed of the $A_0^{(2)}$, $A_{2-}^{(2)}$, $A_{2+}^{(2)}$, $A_{2-}^{(4)}$, $A_{2+}^{(4)}$, $A_{4-}^{(4)}$, and $A_{4+}^{(4)}$ moments.[90] We believe the breaking of cylindrical symmetry is minimized for this system because (i) the molecular beam is at

normal incidence, (ii) the detection is over a large solid angle, centered at normal incidence, and (iii) the residual magnetic field in the ionization region should enforce cylindrical symmetry by causing precession of the angular momentum vectors around the magnetic field direction (the cylindrical symmetry axis).

The quadrupole moment distribution measured for the case of molecular desorption is quite surprising. For rotational states with $J > 12.5$ a positive quadrupole moment is observed. The maximum measured quadrupole moment ($+0.15$) implies that 1.2–1.5[91] times as many molecules desorb with their plane of rotation resembling that of a helicopter (in-plane rotation) as those resembling a cartwheel motion (out-of-plane rotation). Our detection scheme is a measure of number density, not flux. The two quantities are related simply by the velocity of the molecules as they pass through the laser beam. Therefore, any observed alignment may be attributed to an alignment-dependent desorption rate, an alignment-dependent velocity distribution, or a combination thereof. We argue that a molecule's velocity should be relatively independent of the molecule's rotational alignment for the following reasons. The degree of translational accommodation measured for the NO/Pt(111) system at 550 K is unity.[26] In addition, experiments of NO desorbing from Ge[92] and graphite[17] demonstrated that the translational energy distribution appears to be independent of the final rotational level. In order for the alignment-dependent velocity effect to completely account for the observed alignment distribution, the translational temperature for molecules desorbing with a cartwheel motion would have to be 50% higher than that for molecules desorbing with a helicopter motion. We therefore assume that the effect is associated predominantly with an alignment-dependent desorption rate.

The observed alignment cannot be reconciled with the simple picture of a direct transition from the known low-temperature equilibrium position (NO bound normal to the surface through the nitrogen) to the gas phase free rotor without the existence of an intermediate state, occupied immediately prior to desorption. This intermediate state could be a true precursor state or could reflect the anisotropic nature of the top of the (single-minimum) chemisorption well.

Our measurements are most sensitive to the last few interactions the molecule experiences with the surface before desorbing. Calculations by Brenig[93] have found that fast transitions from the bottom of a deep well to the continuum are highly improbable. Hence, we are sensitive to the nature of the molecule–surface potential near the transition state. This idea is corroborated by the following argument.

The dominant mechanism for surface to adsorbate energy transfer is surface vibrational to molecular energy transfer. A surface vibration, however, cannot exert a torque on a molecule adsorbed in an upright configuration which will make it rotate in-plane. Were desorption a direct, impulsive process, we would expect that the desorbed molecules would be aligned to favor cartwheel motion *regardless of J*. If, however, desorption is slow on the time scale of vibrations and requires many surface–molecule collisions during its course, the degrees of freedom of the molecule will be thermally populated as the molecule climbs the chemisorption well. The last surface–molecule interaction releases the molecule from a weakly bound, nearly freely rotating state near the top of the chemisorption well. The result is an isotropic distribution of rotational states. This is what we observe at low to moderate J; indeed, it is what we observe for the majority of the population.

Among the desorbing molecule's degrees of freedom are in-plane and out-of-plane hindered rotations. Since the out-of-plane rotation forces the repulsive O end of NO closer to the surface than the attractive N end, the out-of-plane rotation is more hindered than the in-plane rotation. This could lead to a greater density of states for the in-plane rotation and, therefore, to a net alignment in favor of in-plane rotors.

The following is a plausible explanation of the observed increase in alignment as J increases. This picture draws upon ideas put forth by Bowman and Gossage,[94] and Muhlhausen, Williams, and Tully,[95] which incorporate rotational-to-translational internal conversion, and by Gadzuk *et al.*,[96] which treat a transition from a hindered rotor adsorbed state to the continuum. A second contribution to the energy distribution of desorbing molecules is out-of-plane rotational to translational energy internal conversion. By forcing the repulsive O end of NO toward the surface, an out-of-plane rotation is able to transfer some of its energy into translation. This mechanism becomes progressively more efficient at causing desorption as J increases because more initial out-of-plane rotational energy is available for transfer to translation. An in-plane rotation is ineffective in such a transfer of energy and, thus, will never lose any of its energy to translation. The effect of out-of-plane rotational to translational coupling is to deplete the high end of the rotational distribution through desorption faster than it can be populated by energy transfer from the surface. This mechanism of anisotropic rotational cooling is analogous to that proposed by Tully to describe translational cooling.[47] Furthermore, Muhlhausen, Williams, and Tully[95] predicted a preference for in-plane rotational alignment, though they did not make any predictions for its J dependence.

The observed rotational alignment distribution for molecular desorption is not inconsistent with the NO/Pt(111) measurements of Ertl, Walther, and co-workers[24] and Mantell, Cavanagh, and King.[43] The first group measured no detectable change in the populations extracted from Q branch excitations relative to those of P and R branches.[24] This is a relatively insensitive measure of rotational alignment and the magnitude of their error bars preclude a quantitative determination of the quadrupole moment. Additionally, the maximum rotational quantum state which they were able to observe was $J = 23.5$. The latter study of Mantell *et al.* imposed the following limit on the quadrupole moment: $A_0^{(2)}(J) < |0.1|$ for $J = 4.5$ and $J = 12.5$.[43] This agrees well with our reported value of $A_0^{(2)}(J) = 0.0 \pm 0.04$ for these two quantum levels. Additionally, the experiments of Mantell *et al.*[43] were performed at a much higher coverage and lower temperature than those reported here. At higher coverages, lateral interactions become important and these may inhibit rotational motion in the plane parallel to the surface.

Rotational state-specific measurements in both inelastic scattering and trapping/desorption regimes have provided us with new insight into the basic mechanisms and dynamics of energy transfer processes at surfaces. In past work, the measurement of rotational populations has led to a general sense of energy accommodation on surfaces. In the present work, we have found evidence for an alignment-dependent desorption rate. This leads to a net alignment of desorbed molecules which favors helicopter motion at high (>14.5) J. Rotational alignment measurements are, thus, sensitive to the orientational anisotropies in the molecule–surface potential. The trajectory calculations of the accompanying paper[83] bring this to light.

ACKNOWLEDGMENTS

We would like to thank Glenn D. Kubiak for helpful comments on an early draft of this work. This work was supported by the Office of Naval Research (N00014-87-K-0265). K. W. K. gratefully acknowledges support from the W. R. Grace Foundation. S. F. S. gratefully acknowledges support from a National Science Foundation Graduate Fellowship and from AT&T Bell Laboratories.

[1]M. P. D'Evelyn and R. J. Madix, Surf. Sci. Rep. **3**, 413 (1983).
[2]J. A. Barker and D. J. Auerbach, Surf. Sci. Rep. **4**, 1 (1985).
[3]M. C. Lin and G. Ertl, Annu. Rev. Phys. Chem. **37**, 587 (1986).
[4]R. B. Gerber, Chem. Rev. **87**, 29 (1987).
[5]G. M. McClelland, G. D. Kubiak, H. G. Rennagel, and R. N. Zare, Phys. Rev. Lett. **46**, 831 (1981).
[6]G. D. Kubiak, J. E. Hurst, Jr., H. G. Rennagel, G. M. McClelland, and R. N. Zare, J. Chem. Phys. **79**, 5163 (1983).
[7]A. W. Kleyn, A. C. Luntz, and D. J. Auerbach, Phys. Rev. Lett. **47**, 1169 (1981).
[8]A. C. Luntz, A. W. Kleyn, and D. J. Auerbach, J. Chem. Phys. **76**, 737 (1982).
[9]A. C. Luntz, A. W. Kleyn, and D. J. Auerbach, Phys. Rev. B **25**, 4273 (1982).
[10]A. W. Kleyn, A. C. Luntz, and D. J. Auerbach, Surf. Sci. **117**, 33 (1982).
[11]A. W. Kleyn, A. C. Luntz, and D. J. Auerbach, Surf. Sci. **152**, 99 (1985).
[12]J. Misewich and M. M. T. Loy, J. Chem. Phys. **84**, 1939 (1986).
[13]J. S. Hayden and G. J. Diebold, J. Chem. Phys. **77**, 4767 (1982).
[14]A. Mödl, H. Robota, J. Segner, W. Vielhaber, M. C. Lin, and G. Ertl, J. Chem. Phys. **83**, 4800 (1985).
[15]F. Frenkel, J. Häger, W. Krieger, H. Walther, G. Ertl, J. Segner, and W. Vielhaber, Chem. Phys. Lett. **90**, 225 (1982).
[16]J. Häger and H. Walther, J. Vac. Sci. Technol. B **3**, 1490 (1985).
[17]J. Häger, Y. Shen, and H. Walther, Phys. Rev. A **31**, 1962 (1985).
[18]R. J. Hamers, P. L. Houston, and R. P. Merrill, J. Chem. Phys. **83**, 6045 (1985).
[19]R. J. Hamers, P. L. Houston, and R. P. Merrill, J. Chem. Phys. **88**, 6548 (1988).
[20]J. Misewich, H. Zacharias, and M. M. T. Loy, J. Vac. Sci. Technol. B **3**, 1474 (1985).
[21]J. Misewich, H. Zacharias, and M. M. T. Loy, Phys. Rev. Lett. **55**, 1919 (1985).
[22]A. V. Hamza, P. M. Ferm, F. Budde, and G. Ertl, Surf. Sci. **199**, 13 (1988).
[23]F. Frenkel, J. Häger, W. Krieger, H. Walther, C. T. Campbell, G. Ertl, H. Kuipers, and J. Segner, Phys. Rev. Lett. **46**, 152 (1981).
[24]J. Segner, H. Robota, W. Vielhaber, G. Ertl, F. Frenkel, J. Häger, W. Krieger, and H. Walther, Surf. Sci. **131**, 273 (1983).
[25]M. Asscher, W. L. Guthrie, T.-H. Lin, and G. A. Somorjai, Phys. Rev. Lett. **49**, 76 (1982).
[26]M. Asscher, W. L. Guthrie, T.-H. Lin, and G. A. Somorjai, J. Chem. Phys. **78**, 6992 (1983).
[27]D. C. Jacobs, K. W. Kolasinski, R. J. Madix, and R. N. Zare, J. Chem. Phys. **87**, 5038 (1987).
[28]E. Kolodney, D. Baugh, P. S. Powers, H. Reisler, and C. Wittig, Chem. Phys. Lett. **145**, 177 (1988).
[29]J. W. Hepburn, F. J. Northrup, G. L. Ogram, J. C. Polanyi, and J. M. Williams, Chem. Phys. Lett. **85**, 127 (1982).
[30]D. Ettinger, K. Honma, M. Keil, and J. C. Polanyi, Chem. Phys. Lett. **87**, 413 (1982).
[31]J. B. Cross and J. B. Lurie, Chem. Phys. Lett. **100**, 174 (1983).
[32]B. D. Kay and T. D. Raymond, Chem. Phys. Lett. **130**, 79 (1986).
[33]B. D. Kay and T. D. Raymond, J. Chem. Phys. **85**, 4140 (1986).
[34]B. D. Kay, T. D. Raymond, and M. E. Coltrin, Phys. Rev. B **36**, 6695 (1987).
[35]D. S. Y. Hsu, M. A. Hoffbrauer, and M. C. Lin, Surf. Sci. **184**, 25 (1987).
[36]D. S. Y. Hsu and M. C. Lin, J. Chem. Phys. **88**, 432 (1988).
[37]G. O. Sitz, A. C. Kummel, and R. N. Zare, J. Vac. Sci. Technol. A **5**, 513 (1987).
[38]G. O. Sitz, A. C. Kummel, and R. N. Zare, J. Chem. Phys. **87**, 3247 (1987).
[39]G. O. Sitz, A. C. Kummel, and R. N. Zare, J. Chem. Phys. **89**, 2558 (1988).
[40]R. R. Cavanagh and D. S. King, Phys. Rev. Lett. **47**, 1829 (1981).
[41]D. S. King and R. R. Cavanagh, J. Chem. Phys. **76**, 5634 (1982).
[42]D. S. King, D. A. Mantell, and R. R. Cavanagh, J. Chem. Phys. **82**, 1046 (1985).
[43]D. A. Mantell, R. R. Cavanagh, and D. S. King, J. Chem. Phys. **84**, 5131 (1986).
[44]W. H. Weinberg and R. P. Merrill, J. Chem. Phys. **56**, 2881 (1972).
[45]J. C. Polanyi and R. J. Wolf, J. Chem. Phys. **82**, 1555 (1985).
[46]J. Häger and H. Walther, J. Vac. Sci. Technol. B **3**, 1490 (1985).
[47]J. C. Tully, Surf. Sci. **111**, 461 (1981).
[48]E. K. Grimmelmann, J. C. Tully, and E. Helfand, J. Chem. Phys. **74**, 5300 (1981).
[49]L. V. Novakoski and G. M. McClelland, Phys. Rev. Lett. **59**, 1259 (1987).
[50]E. W. Kuipers, M. G. Tenner, A. W. Kleyn, and S. Stolte, Nature **334**, 420 (1988).
[51]D. C. Jacobs, R. J. Madix, and R. N. Zare, J. Chem. Phys. **85**, 5469 (1986).
[52]C. M. Comrie, W. H. Weinberg, and R. M. Lambert, Surf. Sci. **57**, 619 (1976).
[53]J. L. Gland and B. A. Sexton, Surf. Sci. **94**, 355 (1980).
[54]R. J. Gorte, L. D. Schmidt, and J. L. Gland, Surf. Sci. **109**, 367 (1981).
[55]B. E. Hayden, Surf. Sci. **131**, 419 (1983).
[56]M. Kiskinova, G. Pirug, and H. P. Bonzel, Surf. Sci. **136**, 285 (1984).
[57]H. Ibach and S. Lehwald, Surf. Sci. **76**, 1 (1978).
[58]M. R. Albert and J. T. Yates, Jr., *The Surface Scientist's Guide to Organometallic Chemistry* (American Chemical Society, Washington, D.C., 1988), p. 36.
[59]R. E. Feltham and J. H. Enemark, in *Topics in Stereochemistry*, edited by G. L. Geoffrey (Wiley, New York, 1988), Vol. 12.
[60]J. A. Serri, M. J. Cardillo, and G. E. Becker, J. Chem. Phys. **77**, 2175 (1982).
[61]T.-H. Lin and G. A. Somorjai, Surf. Sci. **107**, 573 (1981).
[62]C. T. Campbell, G. Ertl, and J. Segner, Surf. Sci. **115**, 309 (1982).
[63]J. A. Serri, J. C. Tully, and M. J. Cardillo, J. Chem. Phys. **79**, 1530 (1983).
[64]K. Kruse, G. Abend, and J. H. Block, J. Chem. Phys. **88**, 1307 (1988).
[65]W. L. Guthrie, T.-H. Lin, S. T. Ceyer, and G. A. Somorjai, J. Chem. Phys. **76**, 6398 (1982).
[66]D. C. Jacobs and R. N. Zare, J. Chem. Phys. **85**, 5457 (1986).
[67]A magnetic field along the cylindrical symmetry axis will not affect the observed alignment. Instead, it will insure that stray transient fields will be insufficient to alter the net field direction.
[68]The major impurities in the sample as determined by our quadrupole mass spectrometer are N_2 and N_2O. N_2O decomposes on platinum to form $N_2(g)$ and $O(a)$. H. G. Linz and L. Reikert, Z. Physik, Chem. **42**, 87 (1964).
[69]The quoted rotational temperature represents only the rotational states with $J<7.5$. A greater "temperature" is observed for states of higher J.
[70]D. Golomb, R. E. Good, and R. F. Brown, J. Chem. Phys. **52**, 1545 (1970).
[71]Below 190 K, NO begins to fill the disordered sites, as evidenced by the thermal desorption spectra and LEED data.
[72]Sticking is defined as the collisional process that leads to an adsorbed molecule as its end result. If, however, a saturation coverage is present no further adsorption is possible. Thus, a molecule incident upon a saturated surface cannot "stick." If it is accommodated by the surface it must imme-

diately reenter the gas phase. This process of accommodation that does not lead to adsorption is called trapping. Trapping is also commonly used to describe the process of entering into a precursor state.

[73]C. H. Greene and R. N. Zare, J. Chem. Phys. **78**, 6741 (1983).

[74]High-resolution two-color photoelectron angular distributions have determined that large variations in the intermediate state alignment affect the ionization cross section by less than 10%. S. W. Allendorf, D. J. Leahy, D. C. Jacobs, and R. N. Zare, J. Chem. Phys. (in press).

[75]This assumes that the system exhibits cylindrical symmetry.

[76]Normal incidence/normal detection prohibits angular discrimination against the incident molecular beam. Temporal discrimination is also impossible because of the slow falling edge on the molecular beam pulse relative to the flight time of the molecules (0.5 mm/μs). However, due to the low rotational temperature of the beam, interference from the beam will only affect the states $J < 7.5$.

[77]J. E. Hurst, Jr., G. D. Kubiak, and R. N. Zare, Chem. Phys. Lett. **93**, 235 (1982).

[78]M. H. Alexander *et al.*, J. Chem. Phys. **89**, 1749 (1988).

[79]Comparison of the Boltzmann plots for the $^2\Pi$ states is made by including both rotational and spin–orbit energy in the x-axis.

[80]The nozzle pulse is characterized by a fast rising edge and a relatively slow trailing edge. Care is taken to insure that the laser fires well after the visible tail of the pulse.

[81]G. E. Korzeniewski, E. Hood, and H. Metiu, J. Vac. Sci. Technol. **20**, 594 (1982).

[82]G. E. Korzeniewski, E. Hood, and H. Metiu, J. Chem. Phys. **80**, 6247 (1984).

[83]D. C. Jacobs and R. N. Zare, J. Chem. Phys. **91**, 3196 (1989).

[84]P. Clausing, Ann. Phys. **4**, 533 (1930).

[85]E. P. Wenaas, J. Chem. Phys. **54**, 376 (1971).

[86]The principle of reciprocity can be described as a consequence of time reversal invariance while the principle of detailed balance requires both time reversal invariance and invariance under reflection of spatial coordinates. See Ref. 84 for a more thorough discussion.

[87]R. L. Palmer, J. N. Smith, Jr., H. Saltsburg, and D. R. O'Keefe, J. Chem. Phys. **53**, 1666 (1970).

[88]D. J. Auerbach and C. T. Rettner (private communication).

[89]C. T. Rettner, E. K. Schweizer, and C. B. Mullins, J. Chem. Phys. **90**, 3800 (1989).

[90]A. C. Kummel, G. O. Sitz, and R. N. Zare, J. Chem. Phys. **88**, 6707 (1988).

[91]The limiting values of this range assume that the rotational alignment distribution is best described by either an ellipsoid or a function, which contains a linear combination of $\cos^2\theta$ and $\sin^2\theta$, respectively. The trajectory calculations suggest that the latter function provides a more accurate description of the distribution. In any case, these two functional forms probably represent the limiting cases for the alignment distribution.

[92]T. Gritch, F. Budde, T. J. Chuang, and G. Ertl, Phys. Rev. Lett. **57**, 384 (1986).

[93]W. Brenig, Z. Phys. B **48**, 127 (1982).

[94]J. M. Bowman and J. L. Gossage, Chem. Phys. Lett. **96**, 481 (1983).

[95]C. W. Muhlhausen, L. R. Williams, and J. C. Tully, J. Chem. Phys. **83**, 2594 (1985).

[96]J. W. Gadzuk, U. Landman, E. J. Kuster, C. L. Cleveland, and R. N. Barnett, Phys. Rev. Lett. **49**, 426 (1982).